This is the peer-reviewed, final accepted version for American Mineralogist, published by the Mineralogical Society of America.
The published version is subject to change. Cite as Authors (Year) Title. American Mineralogist, in press.
DOI: https://doi.org/10.2138/am-2021-7768. http://www.minsocam.org/

Revision 1, Dec 9, 2020 **Word Count 9888**

Pseudomorphic 9-line silician ferrihydrite and Fe-rich serpentine-group minerals in FeTi-oxide rich ferroan peridotite, Laramie anorthosite complex, Wyoming, U.S.A.

BERNARD W. EVANS[1], SCOTT M. KUEHNER[1] and DAVID J. JOSWIAK[2]

[1]Department of Earth and Space Sciences, University of Washington, Seattle, WA 98195-1310, U.S.A.

[2]Department of Astronomy, University of Washington, Seattle, WA 98195-1580, U.S.A.

ABSTRACT

Low-temperature hydrous alteration of FeTi-oxide-rich ferroan peridotite, Laramie anorthosite complex, Wyoming, produced silician ferrihydrite, cronstedtite, greenalite, hisingerite, and talc. Ferrihydrite occurs as nanocrystals in ~ 50 nm diameter granules that form monomineralic masses up to 300 μm across. It is inferred to have formed by replacement of an igneous sulfide such as pyrrhotite. Electron diffraction shows the ferrihydrite to be a 9-line variety. Si-rich cronstedtite formed thin rims around the ferrihydrite, and talc grew patchily around the cronstedtite. Greenalite formed in ~10 μm cracks through all the above minerals and olivine, and hisingerite microveinlets partially replaced olivine. Igneous minerals remaining include olivine Fa_{46}, magnetite, ilmenite, hornblende, biotite, and trace clinopyroxene. Correlations among the constituents of ferrihydrite determined by electron-microprobe, including anhydrous totals, indicate progress during growth of two charge-balanced exchanges involving silica enrichment: an inverse cronstedtite substitution $(MgFe^{2+},Si)(Fe^{3+}Mn^{3+})_{-2}$ and an inverse hydrogarnet substitution SiH_{-4}. The cronstedtite exchange requires charge and size balance

across nearest-neighbor *T* and *O* crystal sites, suggesting crystal-interior rather than crystal-surface control. Ferrihydrite's composition reflects time- and space-related variations in the chemical potentials of components in the hydrous fluid at the site of alteration. An upper limit for SiO_2 of 14 – 15 wt.%, or ≈ 1.0 Si per 5-cation formula unit, would seem to correspond to the limit of availability in ferrihydrite of tetrahedral sites open to the entry of Si. Projected to zero SiO_2, our EPMA data indicate an anhydrous total of ≈ 83 wt.% for end-member ferrihydrite, a number that matches the formula: $Fe_{10}O_{15}{\cdot}9H_2O$. The geochemical properties of Laramie ferrihydrite are shared by some samples of altered chondritic and Martian meteorites. Ferrihydrite on Earth commonly occurs as a surface deposit; unlike the Laramie occurrence, these lack the microspatial coherence of replacements/pseudomorphs to show systematic, structure-related element variations. The superior crystal quality of the Laramie ferrihydrite likely contributed to its unique compositional variability.

Keywords: ferrihydrite, element correlations, cronstedtite, hydrogarnet, Laramie peridotite, Keggin cluster

INTRODUCTION

Ferrihydrite was characterized as a mineral by Towe and Bradley (1967), named as such by Chukhrov et al. (1971, 1974), and approved shortly after by the IMA (Fleischer et al. 1975). As reviewed in Childs (1992) and Jambor and Dutrizac (1998), ferrihydrite is a nanocrystalline ferric oxyhydroxide occurring on Earth as reddish-brown films and crusts in surface waters, stream and lake sediments, soils of many kinds, acid mine wastes and drainage, fumaroles, hot

and cold springs, and sea-floor hydrothermal systems (e.g., early work by Henmi et al. 1980; Carlson and Schwertmann 1981; Wilson and Russell 1983; Childs et al. 1982, 1986; Schwertmann et al. 1987; Schwertmann 1988). Extraterrestrial ferrihydrite was discovered in the chondrites Orgueil (Tomeoka and Buseck 1988), Kakangari (Brearley 1989) and Vigarano (Lee et al. 1996), and the Nilpena ureilite (Brearley and Prinz 1992), Martian nakhlites (Treiman et al. 1993; Lee et al. 2015), and in interplanetary dust particles (Matrajt et al. 2002; Nakamura et al. 2004). It may well be present on the surface of Mars (Dehouk et al. 2017). Ferrihydrite is typically a precipitate from an iron-rich aqueous fluid resulting from the supergene decomposition of sulfide ore minerals, and its growth in some cases is mediated by lichen or bacteria (Chukhrov et al. 1974; Cornell and Schwertmann 1979; Burford et al. 2003; Kim and Kim 2003; Toner et al. 2009; Lartaud et al. 2011). In some instances, including the Laramie example, it is pseudomorphic after the source mineral, so element transport attending its growth was minimal; in other cases (spring and river waters) transport of iron is kilometric in scale.

Principal components of ferrihydrite are iron, oxygen, and hydrogen. The mineral has an ephemeral existence in nature, altering with geologic time to more stable goethite (as revealed by TEM in the Laramie occurrence, see below) and hematite (Chukhrov et al. 1974; Schwertmann and Murad 1983; Cornell et al. 1987; Childs 1992; Jiang et al. 2018). The particle size of natural and synthetic ferrihydrite varies in the range 3 to 10 nm (Jambor and Dutrizak 1998), thus providing coherent-scattering domain sizes marginally sufficient for quality X-ray diffraction patterns. These are conventionally labeled after the number of peaks: for example “2-line” or 2L ferrihydrite with two broad reflections, or patterns with sharp “6-line” or “7-line” (6L, 7L) peaks (Schwertmann 1988; Eggleton and Fitzpatrick 1988; Konishi et al. 2012), the 6-line being consistent with the 1975 IMA definition of ferrihydrite (Janney et al. 2001). A structurally

coherent size of 20-60 domains of Fe,O,OH,H_2O per particle was estimated by Childs (1992). As a nanomineral it is a phase with a very-large relative surface area, equivalent to as much as 35% of its volume according to Jambor and Dutrizac (1998), and so its bulk chemical composition integrates surface and interior properties. These properties create ambiguity with respect to its chemical formula and the structural role of some elements, for example, silicon (e.g., Cornell et al. 1987; Cismasu et al. 2011). Its large surface area and great reactivity on the other hand make it a mineral with important applications as an industrial adsorbent.

The chemical formula of this nominally simple-system (Fe-O-H) mineral has challenged workers since its discovery, the problems being its content of OH and H_2O, and the role of adsorbed and, in nature, possible additional elements. Formula proposals have been offered by Towe and Bradley (1967), Chukhrov et al. (1971, 1974), Fleischer et al. (1975), Russell (1979), Eggleton and Fitzpatrick (1988), Jambor and Dutrizac (1998), Boyd and Scott (1999), Hiemstra and Van Riemsdijk (2009), Michel et al. (2007, 2010), and Hiemstra (2013). A valid formula fundamentally requires, among other things, supporting high-quality crystal-structure information, based on diffraction and spectroscopy; however the issue has not acquired a great level of unanimity in the nanomineral community.

Eggleton and Fitzpatrick (1988; 1990) proposed a sheet structure for ferrihydrite with 2/3 octahedral and 1/3 atoms of tetrahedral iron. Their model was challenged by Manceau et al. (1990), Pankhurst and Pollard (1992) and by Drits et al. (1993). Drits et al. (1993) concluded that ferrihydrite consists of a basically defect-free component "f" (hexagonal with a = 0.296 nm and c = 0.940 nm), a defective component ("d") and ultradispersed hematite. In the defect-free component, a close-packed arrangement of oxygen and hydroxyl layer fragments supports octahedral sites 50% occupied by Fe. Using EXAFS and XANES, Zhao et al. (1994) concluded

that as much as 25% of Fe ions could be tetrahedral but only at the particle surface. Also, it emerged that the "aging" of synthetic ferrihydrite, including the degree of dehydroxylation at its surface, could influence iron coordination and the lengths and edge and corner linkages of the core octahedral chains. Janney et al. (2000ab, 2001) found that, in addition to particle size, there are structural differences between 2L and 6L ferrihydrite, and that the structure of 6L ferrihydrite is similar to "defect-free" ferrihydrite. A neutron diffraction study by Jansen et al. (2002) found support for the "f" and "d" component model of ferrihydrite (Drits et al. 1993), but not for the presence of hematite.

In contrast to previous studies, Michel et al. (2007) argued for a "single-phase" Keggin-based structural model for ferrihydrite using the PDF method (pair distribution function) for analyzing total X-ray scattering data. Keggin structures are stable polyoxometalate anion clusters long known as assembling in acidic aqueous solutions and consisting of a central tetrahedral anion caged inside twelve octahedra. According to Michel et al. (2007), ferrihydrite is composed of 2 – 6 nm domains, is hexagonal $P6_3mc$, with a unit cell $a \sim 0.595$ nm and $c = 0.906$ nm, and possesses a chemical formula of $Fe_{10}O_{14}(OH)_2$ making it isostructural to the mineral akdalaite, $Al_{10}O_{14}(OH)_2$. Not shown in this formula is the likely presence of particle-size dependent, surface-bound water. The structure in its ideal form (larger particles) consists of 20% FeO_4 and 80% FeO_6 polyhedra according to Michel et al. (2007). The corresponding layered structure is illustrated in Hiemstra (2013, Fig. 1). It has recently become accepted that, instead of atom-by-atom growth, the iron oxide minerals form by the aggregation of tiny precursor iron-oxygen clusters (Banfield et al. 2000; Baumgartner et al. 2013). In support of this model, Sadeghi et al. (2015) and Weatherill et al. (2016) showed that the growth of synthetic ferrihydrite starts with the nucleation of Fe^{3+} monomers with ~ 0.45 nm radius Fe_{13} Keggin clusters. These subsequently

aggregate into ~ 3 nm diameter 2-line ferrihydrite particles in which the Keggin motif is preserved. It is not entirely clear, however, if this formation pathway is applicable to the natural environment (Weatherill et al. 2016), especially to ferrihydrite produced by mineral replacement. Further three-dimensional aggregation of such nucleation clusters (e.g. to particles approaching 10 nm in diameter) is evidently difficult. In contrast to sheet silicates like cronstedtite, lizardite, and talc that can extend in classical fashion, ferrihydrite is unable to grow beyond the nanoscale.

The question of the presence or otherwise of core $^{IV}Fe^{3+}$ polyhedra in ferrihydrite apparently remains to this day. It is an issue that has generated a great deal of diffraction and spectrographic work (XRD, XANES, EXAFS, EELS, Mössbauer, XAS, XMCD, SAED), seemingly conflicting results, and ongoing discussion. All investigators have worked on synthetic material. Supporters of modest proportions of essential $^{IV}Fe^{3+}$, along with Eggleton and Fitzpatrick (1988, 1990), have been Michel et al. (2007, 2010), Parise et al. (2010), Xu et al. (2011), Harrington et al. (2011), Maillot et al. (2011), Guyodo et al. (2012), Hocking et al. (2012), Peak and Regier (2012a,b) and Hiemstra (2013). The zero $^{IV}Fe^{3+}$ view has been expressed by Combes et al. (1989, 1990), Manceau et al. (1990), Drits et al. (1993), Manceau and Drits (1993), Rancourt and Meunier (2008), Marchand and Rancourt (2009), Manceau (2009, 2010, 2011, 2012a,b), Manceau et al. (2014), Hiemstra and Riemsdijk (2009) and Paktunc et al. (2013). In this paper we hope to stimulate new thoughts based on the geochemical properties of ferrihydrite in a peridotite.

There are currently two formulae for ferrihydrite on the table for critical users. They differ in their acceptance or otherwise of tetrahedral ferric iron. One accommodates 20% of tetrahedral Fe^{3+}, making it an analog of akdalaite $Al_{10}O_{14}(OH)_2$. The other lacks $^{IV}Fe^{3+}$ making it

an analog of akaganeite $(Fe^{3+}Ni^{2+})_8(OH,O)_{16}Cl_{1.25}$. IMA has accepted the akdalaite formula, namely $Fe_{10}O_{14}(OH)_2$. At face value, this formula has a non-volatile content of 98.7%.

Notably absent from the standard formulae for ferrihydrite is silicon, which is commonly present (Fig. 1) at levels ranging from 5 to 14 wt.% SiO_2 in analyses of terrestrial and extra-terrestrial ferrihydrite. The reluctance to include silicon in the standard formula derives from uncertainty as to whether some or all of the Si is adsorbed at the surface and is not "in the structure". The fact that a portion of the Si can be extracted (i.e. is labile) from ferrihydrite with reagents such as NaOH (Carlson and Schwertmann 1981) has supported this view. According to Jambor and Dutrizac (1998, p.2563): "*Silica's*... nonessential character is suggested by the wide variation in percentages of silica (in natural ferrihydrite), and is proved by silica-free syntheses in the laboratory. The syntheses indicate that only Fe, O, and H are necessary…" This view seems to us to be freighted by 50 years of published work on synthesized material and overlooks the requirement that a mineral is by definition a product of nature (cf. Fig.1). Aside from Fe, Mg, Mn, Ni, and Ca (see below), other potential cations and anions (Ti, Al, Na, Cl, P_2O_5, SO_3, and CO_2) figure prominently in some published analyses of ferrihydrite (e.g., Parfitt et al. 1992; Jambor and Dutrizac 1998). However, given the submicroscopic grain-size of most occurrences of ferrihydrite, we have to view with suspicion the acceptability of these components as belonging to ferrihydrite. As we shall see below, Si plays a significant geochemical/structural role in natural ferrihydrite, one that arguably might be recognized in its formula.

LARAMIE FERRIHYDRITE

In the course of an electron microprobe examination of a thin section of 1.43 Ga Laramie complex oxide-rich peridotite ("Oxide Body", Tutolo et al. 2019), the authors encountered,

157 enclosed in olivine, modally small amounts (around 1%) of ≈ 50 to 300 μm diameter masses of
158 highly electron-reflecting material containing predominantly iron and silicon. Initially thought by
159 us to be a high-Fe cronstedtite, a literature search showed instead that analyses of naturally
160 occurring ferrihydrite encompassed our unknown quite well in Si, Fe, Mn and Mg. Our
161 identification of ferrihydrite was subsequently confirmed by selected area electron diffraction
162 (SAED) in a transmission microscope (TEM), as detailed below. The Laramie ferrihydrite is
163 perhaps unusual in that it is a subsurface mineral replacement of primary magmatic sulfides
164 rather than a surface deposit or encrustation, and so it provided an opportunity to collect
165 petrogenetic information based on in-situ, sample-scale spatial relationships in a "rock-forming"
166 ferrihydrite. As a result, we found in our ferrihydrite intriguing correlations and counter-
167 correlations among the concentrations of Si, Mg, Mn, and total-Fe. Such correlations have not
168 been reported in previous accounts of terrestrial ferrihydrite. As discussed below, the correlations
169 are interpreted here as a crystal-chemical response in the ferrihydrite to dissolution and growth at
170 the expense of pyrrhotite or pyrite in a peridotite exposed to a low-temperature hydrous pore-
171 fluid system whose chemical potentials evolved in space and time.

172 Electron microprobe analyses (EPMA) reported here (Table 1) were obtained at the
173 University of Washington Earth and Space Sciences by wavelength-dispersive spectrometry on a
174 JEOL 733 instrument fitted with Geller Version 7 automation, using a library of synthetic and
175 mineral standards. Analytical conditions were 15kV accelerating potential, 3nA beam current,
176 defocused 3μm beam diameter, and counting times needed to reach 0.4% error (1σ) or 40s for
177 minor elements. Concentration dependent statistical counting errors (1σ) are about 0.7% at 12.5
178 ele% Si, 1% at 36 ele% Fe, 25% at 0.2 ele% Mn, and 7% at 0.45 ele% Ca. Raw data were
179 corrected with the CITZAF package.

Suitable ferrihydrite samples for study by transmission electron microscopy (TEM) were obtained from inclusions in olivine by handpicking with a fine-scale stainless-steel probe under an optical microscope. The ferrihydrite was placed between clean glass slides, lightly crushed and embedded with Embed 812 epoxy resin. A Leica Ultracut ultramicrotome was used to cut ~70nm-thick slices which were placed onto 200-mesh Au TEM grids coated with 10nm-thick carbon films. The ferrihydrite samples were examined with Tecnai 200 keV field-emission scanning transmission electron microscopes equipped with energy dispersive X-ray analyzers located in the Materials Analysis Facility of the Molecular Engineering and Sciences Institute and Department of Astronomy at the University of Washington. Selected-area electron diffraction (SAED) patterns were obtained by illumination of ferrihydrite patches to produce partial ring patterns. A central beam blocker was used to prevent underexposure of the diffraction rings. Measured d-spacings from the ring patterns were compared to X-ray diffraction data from the JCPDS Mineral Powder Diffraction File (Bayliss et al. 1980), Jambor and Dutrizac (1998) and Janney et al. (2000) and are shown in Table 2. Prior to obtaining the diffraction patterns, qualitative and quantitative energy dispersive spectra were collected to verify ferrihydrite. An evaporated Al thin-film, produced at the University of Washington, was used for calibration of the camera lengths for the SAED patterns. Estimated errors for the measured d-spacings are approximately 5%.

Our peridotite sample was taken from the Sybille pit, which exposes a FeTi-oxide-rich peridotite in the Sybille monzosyenite, Laramie anorthosite complex, Wyoming. Among our four course-grained samples, this oxide-rich hand-sample is unique in containing ferrihydrite. Igneous minerals in our oxide-rich sample that survived alteration are euhedral olivine Fa_{46} (roughly 40 modal percent), and heavily exsolved intercumulus ilmeno-magnetite and ilmenite

(roughly 50% modal), together with hornblende, biotite, and a trace of clinopyroxene. Hydrous alteration minerals (Fig. 2) include talc (mg#70), cronstedtite, greenalite, hisingerite as microvein replacements of olivine, and ferrihydrite. The hisingerite was analyzed in Tutolo et al. (2019) and shown to be a magnesian variety enriched in silica. The ferrihydrite is a pseudomorphic replacement of a mineral that we infer to have been a sulfide, probably pyrrhotite, there being no detectable Cu or Zn in or around it at the site. The original sulfide was located exclusively inside cumulus olivine. Ferrihydrite appears at low magnification in EPMA beam-scanning images to be finely granular and variably porous, and at high magnification in a field emission scanning electron microscope (FE-SEM) we see that the granules or spheres average around 50 nm across (Fig. 3). TEM images of such ferrihydrite spheres show that they are generally composed of a very large number of spikes, plates, and granules themselves mostly smaller than 10 nm (e.g., Konishi et al. 2012, Figs. 3.3, 3.5). The ferrihydrite masses are surrounded (Fig. 2) by an up to ≈ 50 μm-wide rim of fine-grained random aggregate of platy cronstedtite with somewhat greater porosity than the ferrihydrite. We infer that the cronstedtite is a marginal reaction product of ferrihydrite with a grain-boundary fluid more representative of the higher Mg, Si-potential environment of the surrounding peridotite. Irregular masses of talc intervene consistently between the cronstedtite and the igneous olivine (Fig. 2). Greenalite occurs as veinlets crosscutting cronstedtite and ferrihydrite. We believe it is reasonable to include three of these minerals - ferrihydrite, cronstedtite, and talc - in a micro-spatial distribution of hydrous reaction products that formed across local compositional gradients between former pyrrhotite grains and matrix olivine. Greenalite is locally replaced by hisingerite, but otherwise its timing is not clear.

We obtained selected-area electron diffraction ring patterns (Fig. 4) from two polycrystalline ferrihydrite grains poikilitically enclosed in olivine. Measured d-spacings (Table 2) are consistent with those reported for synthetic 6-line ferrihydrite by Janney et al. (2000b, 2001). Two additional rings observed in the diffraction patterns from both grains whose d-spacings are larger than those reported by Jambor and Dutrizac (1998) and Janney et al. (2000a) are similar to weak reflections observed in ferrihydrite XRD patterns reported by Drits et al. (1993, Fig. 1). Diffraction pattern G5 (Fig. 4a), taken from a ferrihydrite grain that was in contact with the olivine grain boundary, shows an additional ring of 0.52nm. We interpret this ring as a (110) d-spacing of goethite. The diffraction pattern G2 (Fig. 4b) was obtained from a ferrihydrite grain entirely enclosed within olivine. It conspicuously lacks the 0.52nm ring (Fig. 4c) observed in G5, indicating that goethite is not present. Although the 0.41/0.44nm and 0.33/0.35nm rings could represent cronstedtite, the composition of G2 is a perfect match for ferrihydrite alone, as shown by the EDX analysis in Table 1. Any mixture with cronstedtite would noticeably raise its content of MgO. This means that G2 is pure ferrihydrite, and the two additional rings represent ferrihydrite, thus raising ferrihydrite's count of rings to nine. We reiterate that XRD of ferrihydrite has shown traces of peaks at these d-spacings (eg. Drits et al. 1993). These signs of superior crystallinity of ferrihydrite would appear to reflect its unusual petrogenesis in the present case. Our observations suggest that grain G5 likely experienced late-stage interaction with a grain boundary fluid leading to the growth of goethite in G5, whereas the absence of goethite in G2 reflects the lack of communication with late fluids due to its enclosure in olivine.

The average and extremes of composition of the Laramie ferrihydrite obtained by electron microprobe analysis are set down in Table 1. Concentrations of Ti, Al, Cr, and Ni are

This is the peer-reviewed, final accepted version for American Mineralogist, published by the Mineralogical Society of America.
The published version is subject to change. Cite as Authors (Year) Title. American Mineralogist, in press.
DOI: https://doi.org/10.2138/am-2021-7768. http://www.minsocam.org/

sufficiently small that we can reasonably treat our review of compositional variation in terms of the analyzed elements Si, total Fe, Mn, Mg and Ca (Fig. 5). Our 3µm-spot EPMA analyses undoubtedly integrate unknown compositional variability from a very large number of ferrihydrite nanocrystals. Figure 5 shows measured spot-compositions in terms of weight percent oxide, revealing correlations positive and negative among Si, Mg, Fe and Mn. The lowest Si (8.5 wt.% SiO_2) and highest Fe values are found in the centers of the ferrihydrite masses. It is impossible to know for certain how much of the X-ray yield in these microprobe analyses represents elements adsorbed onto ferrihydrite's abundant surfaces, and how much is generated from crystal cores (see below). Twenty-six spot analyses plotted in Figure 5 fall in the range 8.5 to 13.3 wt. SiO_2. Two outlier analyses with SiO_2 values of 15.5 and 16.05 wt.% were excluded from Figure 5 because they are suspected of being admixed with cronstedtite. Figure 5 shows for our ferrihydrite pseudomorphs that a weight percentage increase in SiO_2 is attended by (1) an increase in MgO, and a decrease in $Fe_2O_3^t + Mn_2O_3$, and (2) an increase in the EPMA anhydrous total (top line in Figure 5) from 83.07% (at zero SiO_2) to 86.72% at SiO_2 = 13.3 wt.%. These trends are not an artifact of contamination by goethite. In this case, the analysis totals would extrapolate to 89.9 wt.% when SiO_2 = 0.0 wt.%. Furthermore, no spot-analyses were obtained showing SiO_2 less than 8.5 wt.%, a value marginally smaller than the main SiO_2 concentration between 9 and 12 wt.%. These observations suggest to us that the coherent trends in Figure 5 can be interpreted as intrinsic to the ferrihydrite, and not influenced by goethite contamination as in TEM location G5. The extrapolated SiO_2-free end-member content (Fig. 5) of $Fe_2O_3 + Mn_2O_3$ = 82.81 wt.% (or 82.84 wt.% if we weigh Mn as Fe) is in excellent agreement with 83.12 wt.% Fe_2O_3 in the formulae $Fe_5HO_8 \cdot 4H_2O$ of Towe and Bradley (1967) and $Fe_{10}O_{15} \cdot 9H_2O$ of Fleischer

This is the peer-reviewed, final accepted version for American Mineralogist, published by the Mineralogical Society of America.
The published version is subject to change. Cite as Authors (Year) Title. American Mineralogist, in press.
DOI: https://doi.org/10.2138/am-2021-7768. http://www.minsocam.org/

et al. (1975). Similarly, contamination of the analytical volume by surface adsorbed SiO_2 is unlikely given the correlation of SiO_2 with MgO.

Trend (1) above, namely SiO_2+MgO replacing $Fe_2O_3^t + Mn_2O_3$ (Fig. 5), can be recognized as an inverse *cronstedtite exchange*. An unknown, small amount of Fe^{2+} is included at this stage with Fe^{3+} in the diagram. Exchange (1) replaces heavy Fe^{3+} with light Mg and Si and so should reduce the non-volatile analysis total L-to-R (Fig. 5). Instead, the reverse happens. Trend (2) is accordingly interpreted as an inverse *hydrogarnet exchange*, namely the replacement of H_4O_2 by SiO_2 (36.0 → 60.09 molecular weight). The inverse hydrogarnet exchange can be viewed in the present case as the exchange component SiH_{-4} operating on initially empty tetrahedral sites in the structure. Proton substitution for Si^{4+} in ferrihydrite was considered as a possibility by Michel et al. (2010, p. 2789).

The relative magnitude of exchanges (1) and (2), as expressed by their production of silicon, can in principle be examined without the complex weight constraints of Figure 5 by using a diagram of cation proportions based on the same analytical data. Figure 6 references Fe, Mn, Mg and Si to Σcations = 5.0, in line with end-member ferrihydrite's proposed formula (and the formulas of cronstedtite and serpentine). We recognize that total *formula* cations of ferrihydrite are rendered variable by the hydrogarnet exchange. There are two extreme possibilities for trends of R^{3+} cations in the diagram with respect to x-axis silicon: (1) the inverse cronstedtite exchange, with R^{3+} declining from 5.0 to 3.0 (replaced by Si, Mg and Fe^{2+}), and (2) the inverse hydrogarnet exchange with R^{3+} (diluted by Si) declining from 5.0 to 4.17 (= 5 X 5/6). The relative progress of the two substitutions in the Laramie ferrihydrite is given by the ratio of the two y-axis intercepts between (1) and (2) defined by the line-fit through our analytical data for R^{3+}. Ideally, this exercise requires that Fe_2O_3 be corrected for an unknown small amount of

This is the peer-reviewed, final accepted version for American Mineralogist, published by the Mineralogical Society of America.
The published version is subject to change. Cite as Authors (Year) Title. American Mineralogist, in press.
DOI: https://doi.org/10.2138/am-2021-7768. http://www.minsocam.org/

293 Fe^{2+} that forms along with Mg in exchange (1). We provisionally assume in Figure 6 that Fe^{2+}
294 atoms are as abundant as Mg atoms. Our analytical data then define a line that strikes the y-axis
295 (Si = 1.0) at 3.479 (closer to the Cro line than the hydrogarnet line). In this case the proportions
296 of substitutions are (1) 59.0% and (2) 41.0%. If we had assumed that Fe^{2+} atoms = Mg/4 atoms,
297 the proportions change to (1) 42.0% and (2) 58.0%. Literature analyses provide little guidance on
298 the Fe^{2+} issue. The best we can say is that the two substitutions in the Laramie ferrihydrite are
299 likely quantitatively similar in their contributions to the uptake of Si in the mineral.

300 Although the contribution of crystal surfaces to our electron-probe analyses is unknown,
301 the element correlations basic to the cronstedtite substitution (Fig. 5), as far as we know, are not
302 a feature of surface adsorption of elements in ferrihydrite (Jambor and Dutrizac 1998). The
303 cronstedtite exchange calls for coupled nearest-neighbor octahedral- and tetrahedral-site
304 response, according to well-understood energetic and geometric factors (Bailey 1988). It is a
305 crystal-chemical feature of bulk crystals. The "type" cronstedtite exchange connects sheet-
306 silicates cronstedtite and serpentine. It is known to progress in robust ferromagnesian silicate
307 minerals in crystalline rocks. It has been recorded to be operative in clinopyroxene (Hafner and
308 Huckenholz 1971), metamorphic amphiboles (Robinson et al. 1982), sapphirine (Steffen et al.
309 1984) and phlogopite (Cruciani et al. 1995). Thus, notwithstanding its controversial qualities,
310 ferrihydrite's crystal structure was geochemically controlling in the present case. It enabled the
311 mineral's elemental makeup to respond to compositional changes, in time and space, in an
312 externally imposed enveloping pore-fluid at the site of alteration. Likewise, the hydrogarnet
313 exchange characterizes bulk crystals. It is found in members of the grossular-andradite series
314 occurring in metagabbros, skarns and rodingites. An alternative proton exchange producing silica
315 is $Si(Fe^{3+} + H^{+})_{-1}$ as proposed by Kawazoe et al. (2016) for wadsleyite. This exchange would

presuppose the presence of $Fe^{3+}(OH)_4$ tetrahedra in end-member ferrihydrite. But, unlike hydrogarnet, only one hydrogen ion rather than four is consumed to produce one silicon. The increase in the non-volatile total would therefore be small.

The porous nature of the Laramie ferrihydrite is a primary feature that is consistent with isovolumetric metasomatic replacement (Putnis 2009) of the precursor sulfide. The ferrihydrite in Figure 2 is zoned with the highest contents of Mg and Si at the rim, where it is in contact with cronstedtite, and closest to the enveloping peridotite, the source of the Mg and Si. Cronstedtite and ferrihydrite thus constitute two basically monomineralic zones in a radial diffusion gradient where Mg and Si are being exchanged for iron and sulfur. One or more of these components behaved as a perfectly diffusing "K-component", which is what enables the growth of monomineralic zones (Brady 1977). We have no way of knowing how much the cronstedtite has advanced at the expense of ferrihydrite, but we can reasonably view them as a paragenesis (see below). High-magnification electron-beam scans show that there is very likely some physical mixing on the micron scale along their mutual contact (Fig. 2), but aside from this, the metasomatic mode of origin of ferrihydrite basically ensured a relatively pure (monomineralic) final product.

We have not considered the possible influence of porosity on the EPMA totals. However, the average (Table 1) of 12 analyses of the cronstedtite, whose microtexture, porosity, and hydrous nature, appears to be somewhat similar to that of the ferrihydrite, has an appropriate total of 99.79 wt.% when a calculated formula H_2O content of 10.64 wt.% is added to the anhydrous total. Porosity notwithstanding, our anhydrous EPMA analysis total for Laramie ferrihydrite, when extrapolated SiO_2-free (83.07 wt.%, Fig. 5), is in good agreement with the oxide formula of ferrihydrite: $(Fe_2O_3)_5{\cdot}9H_2O$ (Fleischer et al. 1975; SiO_2 = 82.8 wt.%).

As reviewed earlier here, the presence or absence of Fe on *T*-sites in ferrihydrite is controversial. Operation of the cronstedtite exchange, as our data suggest, not only implies Fe on *T*- as well as the *O*-sites in ferrihydrite, but also seems to point to a limit where the availability of *T*-sites falls to zero, namely in the region of 14 wt.% SiO_2 (Fig. 5) or Si = 1.0 per five total cations (Fig. 6). It is probably no coincidence that this agrees with the same upper limit of 20% Fe^{3+}-sites occupied by Ge in synthetic ferrihydrite (Song et al. 2000; Paktunc et al. 2013). An upper limit of ≈14 wt.% SiO_2 for the Laramie ferrihydrite agrees well with what seems to be the case for the literature analyses (Fig. 1).

EXTRATERRESTRIAL FERRIHYDRITE

Small amounts of ferrihydrite (large in one case, Tomeoka and Buseck 1988) have been described accompanying phyllosilicate alteration in a number of chondritic meteorites. These occurrences resemble our Laramie example in many ways, most significantly in showing the ferrihydrite to be rock-hosted. Chemical analyses (AEM) of 4-line ferrihydrite in the primitive carbonaceous chondrite Acfer 094 (Greshake 1997) show familiar element correlations, notably NiO and MgO with SiO_2 (Fig. 7). Assuming an inverse cronstedtite substitution for this ferrihydrite, the corresponding cation balance: $\Delta Si = \Delta(Mg+Ni+Fe^{2+})$ is short by 50% if Fe^{2+} is not included. Unless the Si substitution is partly balanced by another component, e.g. $4H^+$, the chondrite ferrihydrite contains about 5 or 6 wt.% FeO. The precursor minerals for ferrihydrite in chondrites are viewed to be Ni-pyrrhotite, pentlandite, troilite, magnetite and/or metal (Hutchinson et al. 1987; Tomeoka and Buseck 1988; Brearley 1989; Keller and Buseck 1990a, 1990b; Lee et al. 1996; Tomeoka and Tanimura 2000; Abreau and Brearley 2011). Ferrihydrite has also been reported as an alteration product in nakhlite (Martian) meteorites (Treiman et al. 1993; Treiman and Lindstrom 1997; Lee et al. 2015; Ling and Wang 2015),

NATURAL FERRIHYDRITE

For the formation of ferrihydrite in nature, the length-scale of aqueous iron transport is typically kilometric in the case of "downstream" deposits in lakes, streams, and soils, and around springs. In mine wastes the scale is mostly meters to tens or hundreds of meters. For the in-situ pseudomorphic replacement of pyrrhotite or pyrite, minimal cation transport is required. As a result, in these cases the minor element content of ferrihydrite may show recognizable links to the geochemistry of the host. Thus, ferrihydrite in chondrites Vigarano CV3 and Acfer-094 shows up to 6 wt.% NiO (Lee et al. 1996; Greshake 1997). In ophiolite-hosted mine wastes and in nakhlites, MgO in ferrihydrite varies up to 6 wt.% (Dinelli et al. 1998; Carbone et al. 2016; Treiman et al. 1993; Treiman and Lindstrom 1997; Lee et al. 2015); and MnO can be high on seamount derived ferrihydrite (Boyd and Scott 1999). Conversely, these elements have lower concentrations in downstream ferrihydrite, in lakes and rivers in volcanic or basement terrains (Chukhrov et al. 1974; Henmi et al. 1980; Childs 1992; Childs et al. 1982, 1986, 1990).

Naturally occurring ferrihydrite is not accurately represented by the simple formula in the synthetic system Fe-O-H; minor amounts of Si, Mg, Mn, Ca, Ni, and very likely Fe^{2+}, are real and located on structural sites. Crystal-chemical factors explain why Ni, Mg, and Si co-vary systematically in ferrihydrite in a chondrite, just as Mn, Mg, and Si do in the Laramie peridotite ferrihydrite occurrence. Silicon is present in natural ferrihydrite at levels ranging up to 15 wt.% SiO_2, so it may be argued that silicon provides the charge-balancing leverage for the uptake of Mg, Fe^{2+} and Ni when these constituents are present in the system. These elements potentially contribute to the survival in nature of natural ferrihydrite with respect to otherwise more stable products such as goethite and hematite (Cornell et al. 1987).

This is the peer-reviewed, final accepted version for American Mineralogist, published by the Mineralogical Society of America.
The published version is subject to change. Cite as Authors (Year) Title. American Mineralogist, in press.
DOI: https://doi.org/10.2138/am-2021-7768. http://www.minsocam.org/

CRONSTEDTITE, GREENALITE AND HISINGERITE

Figure 8 shows the compositions of the sheet silicates cronstedtite, greenalite, hisingerite and talc that are present along with ferrihydrite in our Laramie sample. Compared to the ferrihydrite, the cronstedtite rim in the Laramie sample is enriched in Si, Mg and Fe^{2+} and poorer in total iron and in Fe^{3+}. The formula contents of Fe^{2+} and Fe^{3+} of cronstedtite and the greenalite are evaluated for the diagram on the assumption of a cronstedtite exchange with respect to serpentine. Four of our spot analyses (between Si = 1.0 and 1.6, Fig. 8) are interpreted as physical mixtures of ferrihydrite and cronstedtite, resulting from incomplete replacement of the former by the latter within the analyzed volume. Indeed, the sequence from left to right with increasing formula Si-contents across Figure 8 seems to be consistent with the timing of formation of each mineral as judged from the petrography. Hisingerite is observed to have partially replaced greenalite (as well as olivine), and a greenalite vein has cross-cut cronstedtite (Fig. 2). There is also a spatial element to this sequence: former sulfide locations in contrast to purely olivine locations in the sample.

Laramie cronstedtite is relatively siliceous (Table 1); twelve spot analyses fall in the Si range 1.66 to 1.85 per 5.0 total cations (Fig. 8). This content of Si is higher than in most analyses of natural cronstedtite in the literature, which vary from 1.07 to 1.54 Si pfu. At first sight, this is surprising in light of the coexistence of our cronstedtite with the nominally silica-poor ferrihydrite. The chemographic relations of low-temperature minerals in the triangular SiO_2 – $Fe^{3+}O_{1.5}$ – $(Mg,Fe^{2+})O$ compatibility diagram (Fig. 9) hints at a likely explanation. Possible tie-lines in the two-phase field connecting Fh and Cro compositions show that an evolutionary trajectory Fh → Cro starting from Si-rich ferrihydrite might simply bypass lower-Si cronstedtite. Evidently, the chemical potential of pore-fluid silica in the outer, highest SiO_2 parts of the

ferrihydrite mass ($SiO_2 \approx 14$ wt.%), against which the cronstedtite grew, was higher than that associated with "literature" cronstedtite.

Except for opal-A, the triangular compatibility diagram (Fig. 9) models in a schematic fashion all the secondary minerals in our sample, including the patches of talc around the altered sulfide areas (Fig. 2). Hisingerite alteration of olivine in our sample is not preferentially related spatially to the former sulfide areas. As a result, the mutual solubility of greenalite and hisingerite shown in Figure 9 (Tutolo et al., 2019. Fig. 4) fails to show up in our analyses. Our hisingerite is richer in Mg/Fe than hisingerite associated with ore deposits, and as is commonly the case it appears to be silica-rich (Table 1 this work, Tutolo et al. 2019, Fig. 3) compared to ideal hisingerite owing to the presence of interlayered nontronite impurity (for example, Eggleton and Tilley 1998).

PETROGENESIS OF LARAMIE FERRIHYDRITE

Although accessory in modal amount in the present case, the role of ferrihydrite as an alteration product in a crystalline rock is similar to that of many sheet silicates, for example, lizardite in serpentinite, clays in granites and volcanic rocks, etc., and so its inclusion among the rock-forming minerals would seem to be justified (for example, Deer et al. 2013). The Laramie ferrihydrite is fully enclosed in peridotite, so it is *in situ*, as it is in meteorites, and not a surficial mineral in the strict sense, unlike most other known occurrences of terrestrial ferrihydrite. Excluding loss by leaching at the site, no major step of aqueous transport of ferrous iron and other solutes (as in rivers, springs, and fumaroles), and oxidation and precipitation on exposure to air, was involved. This scenario is consistent with the growth of cronstedtite around the perimeter of the ferrihydrite. Shallow underground pore water, slightly acidified by dissolution

This is the peer-reviewed, final accepted version for American Mineralogist, published by the Mineralogical Society of America.
The published version is subject to change. Cite as Authors (Year) Title. American Mineralogist, in press.
DOI: https://doi.org/10.2138/am-2021-7768. http://www.minsocam.org/

of pyrrhotite, served to redistribute elements on site. Laramie ferrihydrite is clearly a pseudomorphic mineral replacement, although it nucleated and grew independently of the host crystal-structure. Sulfide ores are typically the chief source of the iron in surficial ferrihydrite occurrences (Jambor and Dutrizac 1998). The FeTi-oxides in the Laramie peridotite suffered no hydrous alteration. We view the phase boundary between ferrihydrite and rimming cronstedtite as a frozen state of local equilibrium (Brady 1977) in a fluid-hosted binary diffusion gradient established between decomposing sulfide and surrounding peridotite. The large Fh → Cro composition jump in this system (Fig. 9) suggests that the ferrihydrite had reached (at 1.0 Si apfu) the limit of its intrinsic stability.

Contents of Mg, Mn and Fe in the Laramie ferrihydrite as measured by EPMA correlate with silicon (R^2 = 0.60, 0.34, 0.63 respectively) to a degree that would be a challenge to explain if these elements were simply adsorbed onto ferrihydrite surfaces. The cronstedtite exchange in general implies occupation of structural crystallographic sites following the dictates of effective cation size and the preservation of charge balance across adjacent *T* and *O* sites. It is no irony that ferrihydrite's peripheral neighbor (Fig. 2) in the Laramie case is cronstedtite. In addition, we have been able to recognize, in parallel with the cronstedtite exchange, progress of the purely tetrahedral SiH_{-4} exchange, hydrogarnet in reverse. Chemical variation in ferrihydrite is heavily invested in the *T*-site. We do not discount the energetic properties of ferrihydrite's crystal surfaces, but would argue that their chemical manifestations seem to be dwarfed in the present case by those of the interiors. This is perhaps to be explained by its growth by mineral replacement.

The highest measured Si-content of Laramie ferrihydrite at the phase boundary (Fig. 2) with cronstedtite, namely ~14 wt.% SiO_2 (Fig. 5), is matched by a compilation of analyzed

natural ferrihydrite from the literature. Rather than view the match as coincidental, we prefer to interpret these maxima as indicative of a limit to the possible uptake of Si in ferrihydrite. The few analyses of "ferrihydrite" with as much as 30 wt.% SiO_2 (Henmi et al. 1980; Anderson and Benjamin 1985; Jambor and Dutrizac 1998; Gautier et al. 2006) likely represent misidentifications (cronstedtite, greenalite, chamosite?). On a 5-cation basis, what seems to be an upper limit for silicon is 1.0 per 5 total atoms. This would imply a maximum of 20% tetrahedral sites in the structure that, in the absence of Si, could have been occupied as $^{IV}Fe^{3+}$. Can we conclude that geochemistry has ruled on an issue (tetrahedral iron in ferrihydrite) that spectroscopy and diffraction, according to recent published work, has failed to elicit unanimity? The mutual correlation of cations in our ferrihydrite, with its implications for ordering on *T* and *O* sites, has never before been reported in terrestrial ferrihydrite. Such geochemical relationships are going to be more obvious in cases of slow, subsurface mineral replacement (taking place incrementally) than when ferrihydrite forms by spontaneous surface precipitation from a saturated aqueous solution.

Compared to more stable equivalent minerals such as goethite and hematite (plus quartz), ferrihydrite has the advantage (?) of spontaneous *nucleation* from aqueous fluid in clusters. *Growth* of ferrihydrite on the other hand is not accomplished classically atom-by-atom, but by the more complex process of aggregation of clusters. Hence, growth beyond the nanoscale is strongly retarded if not effectively stopped. Time then favors goethite and hematite once they have nucleated. As far as we know, this scenario seems to apply equally to replacement ferrihydrite and ferrihydrite precipitating from surface waters. The uptake of Si and Mg, and attendant volatile decline in the structure of natural ferrihydrite, are thermodynamically

474 stabilizing features. However, the geologic record seems to show that ferrihydrite's survival is
475 nevertheless tenuous (Jambor and Dutrizac 1998).

476 Should consideration perhaps be given to including Si in the standard IMA formula of
477 ferrihydrite? Natural ferrihydrite (as opposed to synthetic ferrihydrite) differs compositionally
478 from goethite and hematite with respect to Si, Mg and probably Fe^{2+}. Our identification of
479 ferrihydrite in the Laramie sample was in fact delayed while we searched mineral databases for
480 one containing Fe, Si, O, and H. We suggest a ferrihydrite formula: $Fe_{4+x}Si_{1-x}O_{7.5}4.5H_2O$. This
481 gives two end-members, a ferrian: (x=1): $Fe_5O_{7.5}4.5H_2O$ and a silician (x=0): $Fe_4SiO_{7.5}.4.5H_2O$.
482 The latter contains one Fe^{2+} (or Mg) atom.

483 **IMPLICATIONS**

484 Ferrihydrite may justifiably be considered as a rock-forming mineral. Its growth as a
485 pseudomorphic replacement of sulfide in a Laramie complex peridotite enabled it to respond to
486 and store a record of time and space variations in the chemical potential of its environment. The
487 uptake of Si in ferrihydrite in the present case is very roughly half controlled by a coupled
488 substitution of elements on *T* and *O* sites, namely: $(Si,MgFe^{2+})(Fe^{3}+)_{-2}$, and the other half relates
489 to an inverse hydrogarnet substitution SiH_{-4}. These variations may have been rendered possible
490 by the unique crystal quality nine-line ferrihydrite. The content of Si appears to have an upper
491 limit of 14-15 wt.% or 20% of total cations. The IMA formula for ferrihydrite should be adjusted
492 to include the elemental substitutions found in terrestrial, subsurface occurrences.

493

494 **ACKNOWLEDGEMENTS**

We thank B.R. Frost, University of Wyoming, for providing peridotite samples from the Laramie complex. S. Guggenheim, D.E. Janney, and A.J. Irving provided helpful comments and criticisms. Michael Kraft, Western Washington University, kindly provided the SEM image Fig. 3. TEM ring patterns were collected with the help of Ellen Lavoie at the Molecular Analysis Facility, a National Nanotechnology Coordinated Infrastructure site at the University of Washington which is supported in part by the National Science Foundation (grant NNCI-1542101), the University of Washington, the Molecular Engineering & Sciences Institute, and the Clean Energy Institute.

REFERENCES

Abreau, N.M. and Brearley, A.J. (2011) Decifering the nebular and asteroidal record in silicates and organic material in the matrix of the reduced CV3 chondrite. Meteoritics and Planetary Science, 46, 2, 252-274.

Anderson, P.R. and Benjamin, M.M. (1985) Effect of silicon on the crystallization and adsorption properties of ferric oxides. Environmental Science and Technology, 19, 1048-1053.

Bailey, S.W. (1988) Structures and compositions of other trioctahedral 1:1 phyllosilicates, Chapter 6 (p. 169--188), in "Hydrous Phyllosilicates (exclusive of micas)", Reviews in Mineralogy, Volume 19, Mineralogical Society of America, editor Paul H. Ribbe.

Banfield, J.F., Welch, S.A., Zhang, H., Ebert, T.T. and Penn, R.L. (2000) Aggregation-based crystal growth and microstructure development in natural iron oxyhydroxide biomineralization products. Science, 289, 751-754.

518 Baumgartner, J., Dey, A., Bomans, P.H.H., Le Coadou, C., Fratzl, P., Sommerdijk, N.A.J.M.
519 and Faivre, D. (2013) Nucleation and growth of magnetite from solution. Nature
520 Materials, 12, 310-314.
521 Bayliss, P., Berry, L.G., Mrose, M.E. and Smith, D.D., editors. JCPDS Mineral Powder
522 Diffraction File Data Book, Swarthmore, PA: JCPDS International Centre for Diffraction
523 Data.
524 Boyd, T.D. and Scott, S.D. (1999) Two-XRD-line ferrihydrite and Fe-Si-Mn oxyhydride
525 mineralization from Franklin Seamount, Western Woodlark Basin, Papua New Guinea.
526 Canadian Mineralogist, 37, 4, 973-990.
527 Brady, J.B. (1977) Metasomatic zones in metamorphic rocks. Geochimica et Cosmochimica
528 Acta, 41, 1, 113-125.
529 Brearley, A.J. (1989) Nature and origin of matrix in the unique type 3 chondrite, Kakangari.
530 Geochimica et Cosmochimica Acta, 53, 2395-2411.
531 Brearley, A.J. and Prinz, M. (1992) CI chondrite-like clasts in the Nilpena polymict ureilite:
532 Implications for aqueous alteration processes in CI chondrites. Geochimica et
533 Cosmochimica Acta, 56, 1373-1386
534 Burford, E.P., Kierens, M., and Gadd, G.M. (2003) Geomycology: fungi in mineral
535 substrates. Mycologist, 17, 3, 98-107.
536 Carbone, C., Marescotti, P., Lucchetti, G., Martinelli, A., Basso, R. and Cauzid, J. (2012)
537 Migration of selected elements of environmental concern from unaltered pyrite-rich
538 mineralizations to Fe-rich alteration crusts. Journal of Geochemical Exploration, 114,
539 109-117.

Carlson, L. and Schwertmann, U. (1981) Natural ferrihydrites in surface deposits from Finland and their association with silica. Geochimica et Cosmochimica Acta, 45, 421-429.

Childs, C.W. (1992) Ferrihydrite: A review of structure, properties and occurrence in relation to soils. Journal of Plant Nutrition and Soil Science, 155, 441-448.

Childs, C.W., Downes, C.J. and Wells, N. (1982) Hydrous iron oxide minerals with short range order deposited in a spring/stream system, Tongariro National Park, New Zealand. Australian Journal of Soil Research, 20, 119-129.

Childs, C.W., Wells, N. and Downes, C.J. (1986) Kokowai Springs, Mt. Egmont, New Zealand: Chemistry and Mineralogy of the ochre (ferrihydrite) deposit and analysis of the waters. Journal of the Royal Society of New Zealand, 16, 85-99. (Q1 R7)

Childs, C.W., Matsue, N. and Yoshinaga, N. (1990) Ferrihydrite deposits in Paddy Races, Aso-Dani. Clay Science, 8, 9-15.

Chukhrov, F.V., Zvyagin, B.B., Gorshkov, A.I., Yermilova, L.P., and Rudnitskaya, E.S. (1971) The Towe-Bradley phase – a product of the supergene alteration of ores. Izvestia Akad Nauk SSSR (Geol Ser.) 1, 3 (in Russian).

Chukhrov, F.V., Zvyagin, B.B., Gorshkov, A.I., Yermilova, L.P. and Balashova, V.V. (1974) Ferrihydrite. International Geology Review, 16, 10, 1131-1143.

Cismasu, A.C., Michel, F.M., Tcaciuc, A.P., Tyliszczak, T. and Brown, G.E. (2011) Composition and structural aspects of naturally occurring ferrihydrite. Comptes Rendus Geoscience, 343, 210-218.

Combes, J.M., Manceau, A., Calas, G., Bottero, J.Y. (1989) Formation of ferric oxides from aqueous solutions: A polyhedral approach by X-ray absorption spectroscopy: I.

563 Hydrolysis and formation of ferric gels. Geochimica et Cosmochimica Acta, 53, 3, 583-
564 594.
565 Combes, J.M., Manceau, A. and Calas, G. (1990) Formation of ferric oxides from aqueous
566 solutions: A polyhedral approach by X-ray absorption spectroscopy: II. Hematite
567 formation from ferric gels. Geochimica et Cosmochimica Acta, 54, 4, 1083-1091.
568 Cornell, R.M. and Schwertmann, U. (1979) Influence of organic anions on the crystallization
569 of ferrihydrite. Clays and Clay Minerals, 27, 402-410.
570 Cornell, R.M., Giovanoli, R. and Schindler, P.W. (1987) Effect of silicate species on the
571 transformation of ferrihydrite into goethite and hematite in alkaline media. Clays and
572 Clay Minerals, 35, 1, 21-28.
573 Cruciani, G., Zanazzi, P.F. and Quartieri, S. (1995) Tetrahedral ferric iron in phlogopite:
574 XANES and Mössbauer compared to single-crystal X-ray data. European Journal of
575 Mineralogy, 7, 255-265.
576 Deer, W.A., Howie, R.A. and Zussman, J. (2013) An introduction to the Rock-Forming
577 Minerals. Third Edition. The Mineralogical Society, London, U.K., 498 p.
578 Dehouk, E., McLennan, S.M., Sklute, E.C. and Dyar, M.D. (2017) Stability and fate of
579 ferrihydrite during episodes of water/rock interactions on early Mars: An experimental
580 approach. Journal of Geophysical Research Planets, 122, 358-382.
581 Dinelli, E., Morandi, N. and Tateo, F. (1998) Fine-grained weathering products in waste
582 disposal from two sulphide mines in the northern Apennines, Italy. Clay Minerals, 33,
583 423-433.
584 Drits, V.A., Sakharov, B.A., Salyn, A.L. and Manceau, A. (1993) Structural models for
585 ferrihydrite. Clay Minerals, 28, 185-207.

586 Eggleton, R.A. and Fitzpatrick, R.W. (1988) New data and a revised structural model for
587 ferrihydrite. Clays and Clay Minerals, 36, 111-124.
588 Eggleton, R.A. and Fitzpatrick, R.W. (1990) New data and a revised structural model for
589 ferrihydrite: Response. Clays and Clay Minerals, 38, 335-336.
590 Eggleton, R.A. and Tilley, D.B. (1998) Hisingerite: a ferric kaolin mineral with curved
591 morphology. Clays and Clay Minerals, 46, 400-413.
592 Fleischer, M., Chao, G.Y. and Kato, A. (1975) New mineral names. American Mineralogist,
593 60, 485-486.
594 Gautier, J., Grosbois, C., Courtine-Nomade, A., Floc, H. and Martin, F. (2006)
595 Transformation of natural As-associated ferrihydrite downstream of a remediated mining
596 site. European Journal of Mineralogy, 18, 187-195.
597 Greshake, A. (1997) The primitive matrix components of the unique carbonaceous chondrite
598 Acfer 094 chondrite: a TEM study. Geochimica et Cosmochimica Acta, 61(2), 437-452.
599 Guyodo, Y., Sainctavit, P., Arrio, M-A., Carvallo, C., Lee Penn, R., Erbs, J.J., Forsberg, B.S.,
600 Morin, G., Maillot, F., Lagroix, F., Bonville, P., Wilhelm, F., and Rogalev, A. (2012) X-
601 ray magnetic circular dichroism provides strong evidence for tetrahedral iron in
602 ferrihydrite. Geochemistry, Geophysics, Geosystems, 13, 6, 1-9.
603 Hafner, S.S. and Huckenholz, H.G. (1971) Mössbauer spectrum of synthetic ferridiopside.
604 Nature, 233, 9-11.
605 Harrington, R., Hausner, D.B., Xu, W., Bhandari, N., Michel, F.M., Brown, G.E. Jr.,
606 Strongin, D.R. and Parise, J.B. (2011) Neutron pair distribution function study of two-
607 line ferrihydrite. Environmental Science and Technology, 45, 9883-9890.

608 Henmi, T., Wells, N., Childs, C.W. and Parfitt, R.L. (1980) Poorly ordered iron-rich
609 precipitates from springs and streams on andesitic volcanoes. Geochimica et
610 Cosmochimica Acta, 44, 365-372.
611 Hiemstra, T. (2013) Surface and mineral structure of ferrihydrite. Geochimica et
612 Cosmochimica Acta, 105, 316-325.
613 Hiemstra, T. and Van Riemsdijk, W.H. (2009) A surface structural model for ferrihydrite I:
614 Sites related to primary charge, molar mass, and mass density. Geochimica et
615 Cosmochimica Acta, 73, 4423-4436.
616 Hocking, R.K., Gates, W.P. and Cashion, J.D. (2012) Comment on "direct observation of
617 tetrahedrally coordinated Fe(III) in ferrihydrite". Environmental Science and Technology,
618 46, 11471-11472.
619 Hutchinson, R., Alexander, C.M.O. and Barber D.J. (1987) The Semarkona meteorite: first
620 recorded occurrence of smectite in an ordinary chondrite. Geochimica et Cosmochimica
621 Acta, 81, 7, 1875-1880.
622 Jambor, J.L. and Dutrizac, J.E. (1998) Occurrence and constitution of natural and synthetic
623 ferrihydrite, a widespread iron oxyhydroxide. Chemical Reviews, 98, 2549-2585.
624 Janney, D.E., Cowley, J.M. and Buseck, P.R. (2000a) Structure of synthetic 2-line ferrihydrite
625 by electron microdiffraction. American Mineralogist, 85, 1180-1187.
626 Janney, D.E., Cowley, J.M. and Buseck, P.R. (2000b) Transmission electron microscopy of
627 synthetic 2- and 6-line ferrihydrite. Clays and Clay Minerals, 48, 111-119.
628 Janney, D.E., Cowley, J.M. and Buseck, P.R. (2001) Structure of synthetic 6-line ferrihydrite
629 by electron nanodiffraction. American Mineralogist, 86, 327-335.

630 Jansen, E., Kyek, A., Schäfer, W. and Schwertmann, U. (2002) The structure of six-line
631 ferrihydrite. Applied Physics A, 74, S1004-S1006.
632 Jiang, Z., Liu, Q., Roberts, A.P., Barrón, V., Torrent, J. and Zang, Q. (2018) A new model for
633 transformation of ferrihydrite to hematite in soils and sediments. Geology, 46(11), 987-
634 990.
635 Kawazoe, T., Chaudhari, A., Smyth, J.R., McCammon, C. (2016) Coupled substitution of
636 Fe^{3+} and H^{+} for Si in wadsleyite: A study by polarized infrared and Mössbauer
637 spectroscopies and single-crystal X-ray diffraction. American Mineralogist, 101, 1236-
638 1239.
639 Keller, L.P. and Buseck, P.R. (1990a) Aqueous alteration in the Kaba CV3 carbonaceous
640 chondrite. Geochimica et Cosmochimica Acta, 54, 2113-2120.
641 Keller, L.P. and Buseck, P.R. (1990b) Matrix mineralogy of the Lancé CO3 carbonaceous
642 chondrite. A transmission electron microscope study. Geochimica et Cosmochimica Acta,
643 54, 1155-1163.
644 Kim, J.J. and Kim, S.J. (2003) Environmental, mineralogical, and genetic characterization of
645 ochreous and white precipitates from acid mine drainage, Taebaeg, Korea. Environmental
646 Science and Technology, 37, 2120-2126.
647 Konishi, H., Xu, H.F. and Guo, H.B. (2012) Nanostructures of natural iron oxide
648 nanoparticles, Chapter 2 in "Nature's Nanostructures" editors Barnard, A.S. and Guo,
649 H.B., 1st. edition, Jenny Stanford Publishing.
650 Lartaud, F., Little, C.T., De Rafelis, M., Bayon, G. Dymont, J., Ildefonse, B. and Le Bris, N.
651 (2011) Fossil evidence for serpentinizing fluids fueling chemosynthetic assemblages.
652 Proceedings of the National Academy of Sciences, 108, 19, 7698-7703.

653 Lee, M.R., Hutchinson, R., and Graham, A.L. (1996) Aqueous alteration in the matrix of the
654 Vigarano (CV3) carbonaceous chondrite. Meteoritics and Planetary Sciences, 31, 4, 477-
655 483.
656 Lee, M.R., Tomkinson, T., Hallis, L.J. and Mark, D.F. (2015) Formation of iddingsite veins in
657 the Martian crust by centripetal replacement of olivine: Evidence from the nakhlite
658 meteorite Lafayette. Geochimica et Cosmochimica Acta, 154, 49-63.
659 Ling, Z. and Wang, A. (2015) Spatial distributions of secondary minerals in the Martian
660 meteorite MIL 03346-168. Journal of Geophysical Research, Planets, 120, 6, 1141-1154.
661 Maillot, F., Morin, G., Yang, Y., Bonnin, D., Ildefonse, P., Chaneac, C. and Calas, G. (2011)
662 New insight into the structure of nanocrystalline ferrihydroxide: EXAFS evidence for
663 tetrahedrally coordinated iron (III). Geochimica et Cosmochimica Acta, 75, 2708-2720.
664 Manceau, A. (2009) Evaluation of the structural model for ferrihydrite derived from real-
665 space modeling of high-energy X-ray diffraction data. Clay Minerals, 44, 19-34.
666 Manceau, A. (2010) PDF analysis of ferrihydrite and the violation of Pauling's principles.
667 Clay Minerals, 45, 225-228.
668 Manceau, A. (2011) Critical evaluation of the revised akdalaite model for ferrihydrite.
669 American Mineralogist, 96, 521-533.
670 Manceau, A. (2012a) Critical evaluation of the revised akdalaite model for ferrihydrite –
671 Reply. American Mineralogist, 97, 255-256.
672 Manceau, A. (2012b) Comment on "Direct observation of tetrahedrally coordinated Fe(III) in
673 ferrihydrite. Environmental Science and Technology, 46, 6882-6884.
674 Manceau, A and Drits,V.A. (1993) Local structure of ferrihydrite and feroxyhite by EXAFS
675 spectroscopy. Clay Minerals, 28, 165-184.

676 Manceau, A., Combes, J.M. and Calas, G. (1990) New data and a revised structural model for
677 ferrihydrite – comment. Clays and Clay Minerals, 38, 331-334.
678 Manceau, A., Skanthakumar, S. and Soderholm, L. (2014) PDF analysis of ferrihydrite:
679 Critical assessment of the under-constrained akdalaite model. American Mineralogist, 99,
680 102-108.
681 Marchand, P. and Rancourt, D.G. (2009) General model for the aqueous precipitation of
682 rough- surface nanocrystals and application to ferrihydrite genesis. American
683 Mineralogist, 94, 1428-1439.
684 Matrajt, G., Joswiak, D., Keller, L. and Brownlee, D. (2002) Could ferrihydrite be a host
685 phase of organics in IDPS? Abstract, Meteoritics and Planetary Science, vol. 37,
686 Supplement, p. A96.
687 Michel, F.M., Ehm, L., Antao, S.M., Lee, P.L., Chopas, P.J., Liu, G., Strongin, D.R.,
688 Schoonen, M.A.A., Phillips, B.L. and Parise, J.B. (2007) The structure of ferrihydrite, a
689 nanocrystalline material. Science, 316, 1726-1729.
690 Michel, F.M., Barrónc, V., Torrent, J, Morales, M.P., Serna, C.J., Boily, J.F., Liu, Q.,
691 Ambrosini, A., Cismasu, A.C. and Brown, G.E. Jr. (2010) Ordered ferrimagnetic form of
692 ferrihydrite reveals links among structure, composition, and magnetism. Proceedings of
693 the National Academy of Science USA, 107, 2787-2792.
694 Nakamura, K., Keller, L.P., Nakamura, T., Noguchi, T. and Zolensky, M.E. (2004)
695 Mineralogical study of hydrated IDPs: X-ray diffraction and Transmission electron
696 microscopy. Lunar and Planetary Science Conference XXXV, abstract #1862.
697 Navrotsky, A., Mazeina, L. and Majzlan, J. (2008) Size-driven structural and thermodynamic
698 complexity in iron oxides. Science, 319 (5870), 1635-1638.

699 Paktunc, D., Manceau, A. and Dutrizac, J. (2013) Incorporation of Ge in ferrihydrite:
700 Implications for the structure of ferrihydrite. American Mineralogist, 98, 848-858.
701 Pankhurst, Q.A. and Pollard, R.J. (1992) Structural and magnetic properties of ferrihydrite.
702 Clays and Clay Minerals, 40, 268-272.
703 Parise, J.B., Harrington, R., Xu, W., Michel, F.M., Hausner, D.B., Debnath, S. and Strongin,
704 D.R. (2010) Understanding the composition and structure of ferrihydrite. Geochimica et
705 Cosmochimica Acta, 74, abstract A793.
706 Parfitt, R.L., Van der Gaast, S.J. and Childs, C.W. (1992) A structural model for natural
707 siliceous ferrihydrite. Clays and Clay Minerals, 40, 6, 675-681.
708 Peak, D. and Regier, T. (2012a) Direct observation of tetrahedrally coordinated Fe(III) in
709 ferrihydrite. Environmental Science and Technology, 46, 3163-3168.
710 Peak, D. and Regier, T. (2012b) Response to comment on “Direct observation of tetrahedrally
711 coordinated Fe(III) in ferrihydrite”. Environmental Science and Technology, 46, 6885-
712 6887.
713 Putnis, A. (2009) Mineral Replacement Reactions, Chapter 3 (p. 87-124) in
714 “Thermodynamics and Mineral Kinetics of Water-Rock Interactions”, Reviews in
715 Mineralogy and Geochemistry, Volume 70(1). Mineralogical Society of America and
716 Geochemical Society, editors E.H.Oelkers and J.Schott.
717 Rancourt, D.J. and Meunier, J.F. (2008) Constraints on structural models of ferrihydrite as a
718 nanocrystalline mineral. American Mineralogist, 93, 1412-1417.
719 Robinson, P., Spear, F.S., Schumacher, J.C., Laird, J., Klein, C., Evans, B.W. and Doolan,
720 B.L. (1982) Phase relations of metamorphic amphiboles: natural occurrence and theory.
721 Chapter 1 (p. 1-227) in “Amphiboles: Petrology and Experimental Phase relations”

722 Reviews in Mineralogy Volume 9B, Mineralogical Society of America, editors
723 D.R.Veblen and P.H.Ribbe.
724 Russell, J.D. (1979) Inferred spectroscopy of ferrihydrite: Evidence for the presence of
725 structural hydroxyl groups. Clay Minerals, 14, 109-113.
726 Sadeghi, O., Zakharov, L.N. and Nyman, M. (2015) Aqueous formation and manipulation of
727 the iron-oxo Keggin ion. Science, 347, issue 6228, 1359-1362.
728 Schwertmann, U. (1988) Occurrence and formation of iron oxides in various
729 pedoenvironments, In "Iron in Soils and Clay Minerals" edited by J.W. Stucki, B.A.
730 Goodman, and U. Schwertmann, eds., NATO ASI (Advanced Science Institute) Series
731 C217, D. Reidel, Dordrecht, Holland, 267-308.
732 Schwertmann, U. and Murad, E. (1983) The effect of pH on the formation of goethite and
733 hematite from ferrihydrite. Clays and Clay Minerals, 31, 277-284.
734 Schwertmann, U., Carlson, L. and Murad, E. (1987) Properties of iron oxides in two Finnish
735 lakes in relation to the environment of their formation. Clays and Clay Minerals, 35, 297-
736 304.
737 Song, Y., Bac, B.H., Lee, Y-B., Kim, M.H., Yoon, W-S., Kim, J.H. and Moon, H-S. (2010)
738 Ge incorporation into 6-line ferrihydrite nanocrystals. CrystEngComm, 12, 1997-2000.
739 Steffen, G., Seifert, F. and Amthauer, G. (1984) Ferric iron in sapphirine: a Mössbauer
740 spectroscopy study. American Mineralogist, 69, 339-345.
741 Tomeoka, K. and Buseck, P.R. (1988) Matrix mineralogy of the Orgueil CI chondritic
742 meteorite. Geochimica et Cosmochimica Acta, 52, 1627-1640.

743 Tomeoka, K. and Tanimura, I. (2000) Phyllosilicate-rich chondrule rims in the Vigarano CV3
744 chondrite: Evidence for parent-body processes. Geochimica et Cosmochimica Acta, 64,
745 11, 1871-1988.
746 Toner, B.M., Santelli, C.M., Marcus, M.A., Wirth, R., Chen, C.S., McCollom, T., Bach, W.
747 and Edwards, K.J. (2009) Biogenic iron oxyhydroxide formation at mid-ocean ridge
748 hydrothermal vents, Juan de Fuca Ridge. Geochimica et Cosmochimica Acta, 73, 388-
749 403.
750 Towe, K.M. and Bradley, W.F. (1967) Mineralogical constitution of colloidal “hydrous
751 ferrous oxides”. Journal of Colloidal Interface Science, 24, 384-392.
752 Treiman, A.H. and Gooding, J.L. (1981) Iddingsite in the Nakhla meteorite: TEM study.
753 Meteoritics abstracts, V.26, 402.
754 Treiman, A.H., Barrett, R.A. and Gooding, J.L. (1993) Preterrestrial aqueous alteration of the
755 Lafayette (SNC) meteorite. Meteoritics, 28, 86-97.
756 Treiman, A.H. and Lindstrom, D.J. (1997) Trace element geochemistry of Martian iddingsite
757 in the Lafayette meteorite. Journal of Geophysical Research, 102, E4, 9153-9163.
758 Tutolo, B.M., Evans, B.W. and Kuehner, S.M. (2019) Serpentine-hisingerite solid solution in
759 altered ferroan peridotite and olivine gabbro. Minerals, 9, 47, 1-14,
760 doi:10.3390/min9010047.
761 Weatherill, J.S., Morris, K., Bots, P., Stawski, T.M., Janssen, A.A., Abrahamsen, L.,
762 Blackham, R. and Shaw, S. (2016) Ferrihydrite formation: The role of Fe_{13} Keggin
763 clusters. Environmental Science and Technology, 50, 9333-9342.
764 Wilson, M.J. and Russell, J.D. (1983) Melanosiderite is siliceous ferrihydrite. Mineralogical
765 Magazine, 47, 85-87.

766 Xu, W., Hausner, D.B., Harrington, R., Lee, P.L., Strongin, D.R. and Parise, J.B. (2011)
767 Structural water in ferrihydrite and constraints this provides on possible structure models.
768 American Mineralogist, 96, 513-520.
769 Zhao, J.M., Huggins, F.E., Feng, Z. and Huffman, G.P. (1994) Ferrihydrite – surface-structure
770 and its effects on phase transformation. Clays and Clay Minerals, 42, 737-746.

771

772 **Text Figures**

773 1) Analyses of Fe, Mn, Mg and Si in terrestrial and extraterrestrial ferrihydrite from the
774 literature (Chukhrov et al. 1974; Henmi et al. 1980; Carlson and Schwertmann 1981;
775 Childs et al. 1982, 1986, 1990; Wilson and Russell 1983; Parfitt et al. 1992; Treiman et
776 al. 1993; Greshake 1997; Dinelli et al. 1998; Boyd and Scott 1999; Kim and Kim 2003).
777 Not included are surficial terrestrial samples with measured phosphate, sulfate, carbonate,
778 or clay impurities.
779 2) Microprobe BSE image of ferrihydrite (Fh) with border of cronstedtite (Cro) in ferroan
780 peridotite "Oxide Body" from the Laramie complex. Talc (Tlc, black) rims Cro.
781 Greenalite (Gre) veins occur in Fh, Cro and olivine (Ol), and hisingerite (His) veins occur
782 in Ol. Bright white phase in veins is magnetite.
783 3) FE-SEM image of spherical masses of ferrihydrite in Laramie peridotite.
784 4) Selected-area electron diffraction TEM ring patterns obtained from two polycrystalline
785 ferrihydrite grains (G5 and G2) located within separate olivines. Measured d-spacings
786 (nm) for each ring are indicated; outer rings (0.28nm and smaller) match ferrihydrite. a)
787 Ring pattern from grain G5 which was located on the edge of the olivine and in contact
788 with the grain boundary displays additional 0.35, 0.44 and 0.52 nm rings. The 0.52 nm

ring is consistent with goethite while the 0.35 nm and 0.44 nm rings could represent goethite and/or cronstedtite. See Table 2. b) Ring pattern from ferrihydrite grain G2 poikilitically enclosed in olivine, without grain boundary contact, displays identical rings as (a) except for the innermost 0.52 nm ring indicating that goethite is not present in G2. c) Expansion of the innermost rings in (b) showing the absence of the 0.52 nm goethite ring. SAED pattern camera lengths: a) CL=300 mm, b) CL=520 mm, c) CL=1000 mm.

5) EPMA spot analyses (24) of oxide components in Laramie ferrihydrite (Fe_2O_3 is total iron), and total anhydrous oxides (uppermost line with zero intercept value of 83.07 wt.%).

6) Electron-probe microanalyses of Fe^{3+} + Mn^{3+} versus Si in Laramie ferrihydrite normalized to 5 total cations. Contents of Fe^{2+} and Mg cations are taken to be the same. Upper and lower lines represent inverse hydrogarnet and inverse cronstedtite exchanges. Not shown: Mg variation: y = 0.332x - 0.058.

7) Positive correlation of NiO and NiO+MgO percent with SiO_2 in chondrite Acfer 094. Data from Greshake (1997).

8) Electron-probe spot analyses of ferrihydrite (Fh) and Fe-rich serpentine-group minerals cronstedtite (Cro), greenalite (Gre), and hisingerite (His), with talc (Tlc) in Laramie oxide-rich peridotite. “Mixed” are compositions likely to be ferrihydrite + cronstedtite not spatially resolved under the electron beam. Cations are normalized to 5.0, a procedure that fails to recognize M-vacancies in hisingerite. FeII and FeIII in ferrihydrite are not separated; they are calculated in cronstedtite and greenalite assuming cronstedtite substitution: $(MgFe^{2+})Si(Fe^{3+})_{-2}$.

9) Schematic illustration of compatibilities of minerals at very low-temperature projected from H_2O into the ternary system SiO_2 - $Fe^{3+}O_{1.5}$ - (Mg,Fe)O, for low levels of Mg. Non is nontronite and Brc is brucite. (e.g. Bogdanov et al. 2008)

This is the peer-reviewed, final accepted version for American Mineralogist, published by the Mineralogical Society of America.
The published version is subject to change. Cite as Authors (Year) Title. American Mineralogist, in press.
DOI: https://doi.org/10.2138/am-2021-7768. http://www.minsocam.org/

Table 1. Chemical Compositions of Laramie Peridotite Minerals

Mineral	Olivine	Lowest-Si Fh	Highest-Si Fh	Average Fh	EDX* Fh	Fh Rims Cro	Veinlet Gre	Ol altn. His
No. of Spots	11	1	1	26	1	12	5	17
Weight Percent								
SiO_2	35.29	8.54	13.33	10.60	11.79	30.80	31.98	43.31
TiO_2	0.03	0.07	0.07	0.07		0.05	0.04	0.01
Al_2O_3	0.01	0.08	0.28	0.13		0.07	0.24	1.29
Cr_2O_3	0.04	0.05	0.05	0.08		0.04	0.03	0.03
Fe_2O_3t		72.92	70.18	72.03	85.28			35.05
FeOt	38.19					43.26	48.23	
MnO	0.55	1.13	0.77	1.01	0.89	0.46	0.21	0.14
MgO	25.58	1.38	2.42	1.83	1.79	13.86	4.53	7.59
NiO	0.06	0.17	0.12	0.10		0.07	0.04	0.05
CaO	0.07	0.67	0.34	0.41	0.29	0.54	1.13	0.96
Anh. Total	99.82	85.01	87.56	86.26	100.0	89.15	86.42	88.43
Formula Cations								
Basis	3 cations	5 cations	5 cations	5 cations	5 cations	5 cations	5 cations	7 anh. ox.
Si	0.999	0.633	0.934	0.766	0.742	1.734	1.979	2.149
Al	0.000	0.007	0.023	0.011		0.004	0.018	0.076
Cr	0.001	0.003	0.006	0.004		0.002	0.002	0.001
FeIIIt		4.070	3.702	3.920	4.019	0.520	0.002	1.309
FeIIt	0.904					1.517	2.495	0.000
Mn	0.013	0.071	0.046	0.062	0.068	0.022	0.011	0.006
Mg	1.079	0.153	0.253	0.197	0.152	1.164	0.418	0.561
Ni	0.001	0.010	0.007	0.006		0.003	0.002	0.002
Ca	0.002	0.053	0.026	0.031	0.026	0.033	0.074	0.051

*Total normalized to 100%.

This is the peer-reviewed, final accepted version for American Mineralogist, published by the Mineralogical Society of America.
The published version is subject to change. Cite as Authors (Year) Title. American Mineralogist, in press.
DOI: https://doi.org/10.2138/am-2021-7768. http://www.minsocam.org/

Table 2: Measured d-spacings and (hkl) planes in this study and comparative literature values for ferrihydrite and goethite.

Row	G2 This study isolated (nm)	G5 This stud grain bnd (nm)	Mineral	Fh Janney et al. (2000a) (nm)	Fh J & D (1998) (nm)	Fh J & D (1998) (hkl)	Goe JCPDS (nm)	Goe JCPDS (hkl)
1	-----	0.52	Goe	-----	-----	-----	0.498	(020)
2	0.41	0.44	Fh, Goe	-----	-----	-----	0.418	(110)
3	0.33	0.35	Fh, Goe	-----	-----	-----	0.338	(120)
4	0.27	0.28	Fh	0.29	-----	-----	-----	-----
5	0.24	0.26	Fh, Goe	0.25	0.252	(110)	0.250	(110)
6	0.22	0.23	Fh, Goe	0.228	0.223 or 0.235	(112) or (004)	0.221	(200)
7	0.19	0.20	Fh, Goe	0.202	-----	-----	0.196	(113)
8	0.175	0.18	Fh, Goe	0.176	0.188 or 0.172	(005) or (114)	0.176	(114)
9	0.167	0.16	Fh, Goe	0.156	0.172 or 0.151	(114) or (115)	0.156	(115)
10	0.13	0.14	Fh, Goe	0.148	0.146	(300)	0.148	(106)

Abbreviations: Fh=ferrihydrite, goe=goethite, bndy=boundary, J & D (1998)=Jambor and Dutrizac (1998), JCPDS=JCPDS International Center for Diffraction Data.

This is the peer-reviewed, final accepted version for American Mineralogist, published by the Mineralogical Society of America.
The published version is subject to change. Cite as Authors (Year) Title. American Mineralogist, in press.
DOI: https://doi.org/10.2138/am-2021-7768. http://www.minsocam.org/

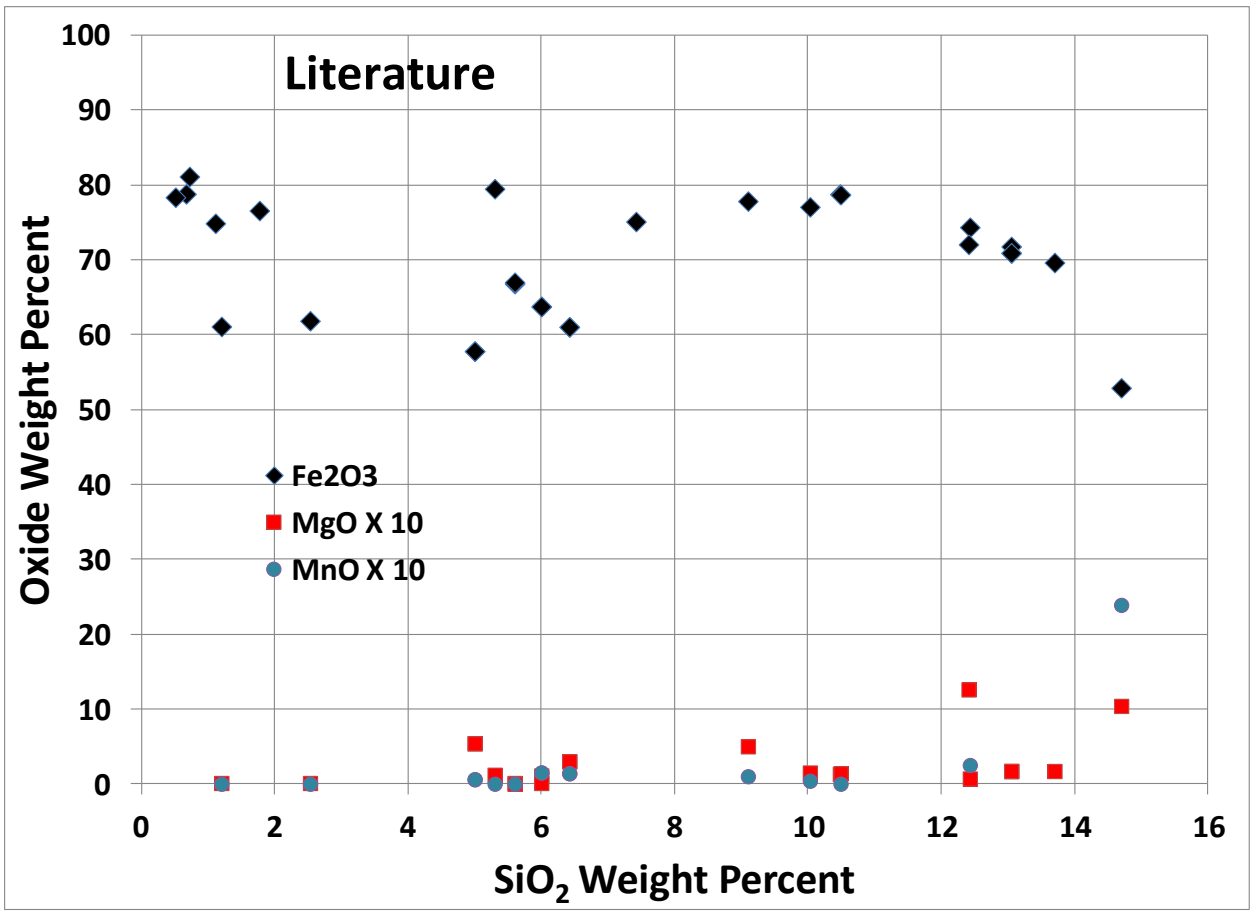

Figure 1

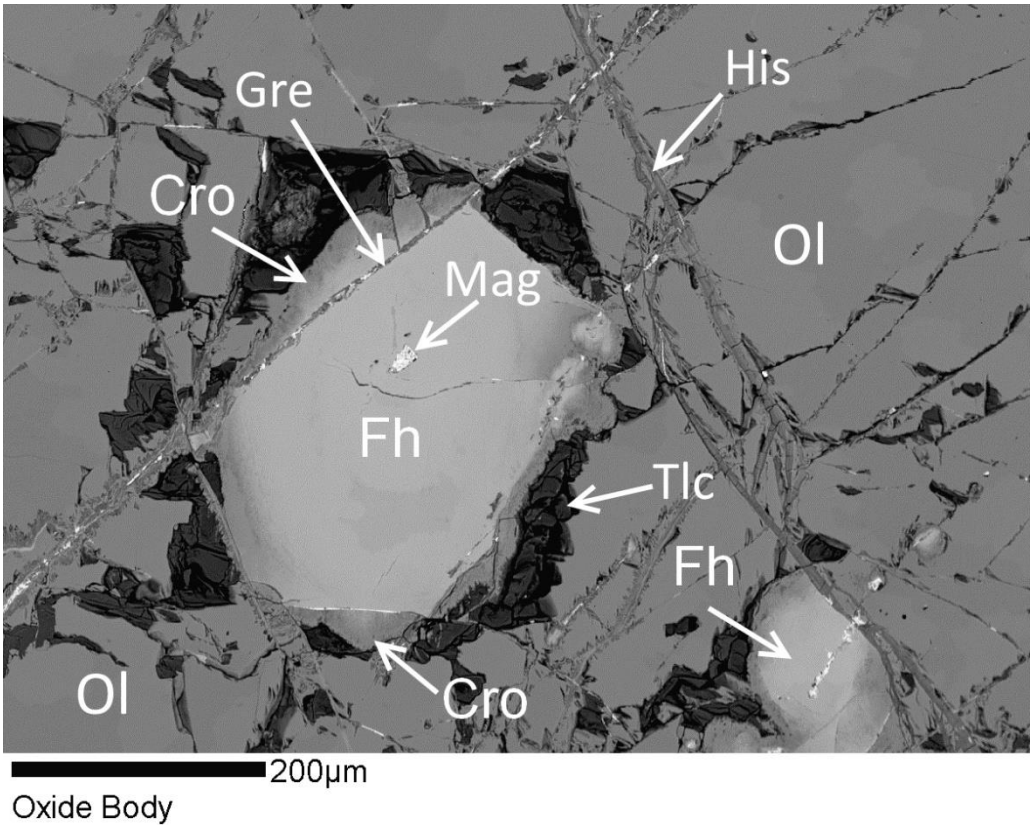

Figure 2

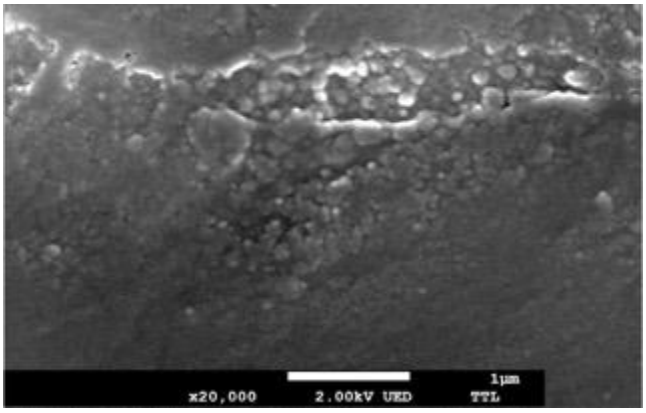

Figure 3

This is the peer-reviewed, final accepted version for American Mineralogist, published by the Mineralogical Society of America.
The published version is subject to change. Cite as Authors (Year) Title. American Mineralogist, in press.
DOI: https://doi.org/10.2138/am-2021-7768. http://www.minsocam.org/

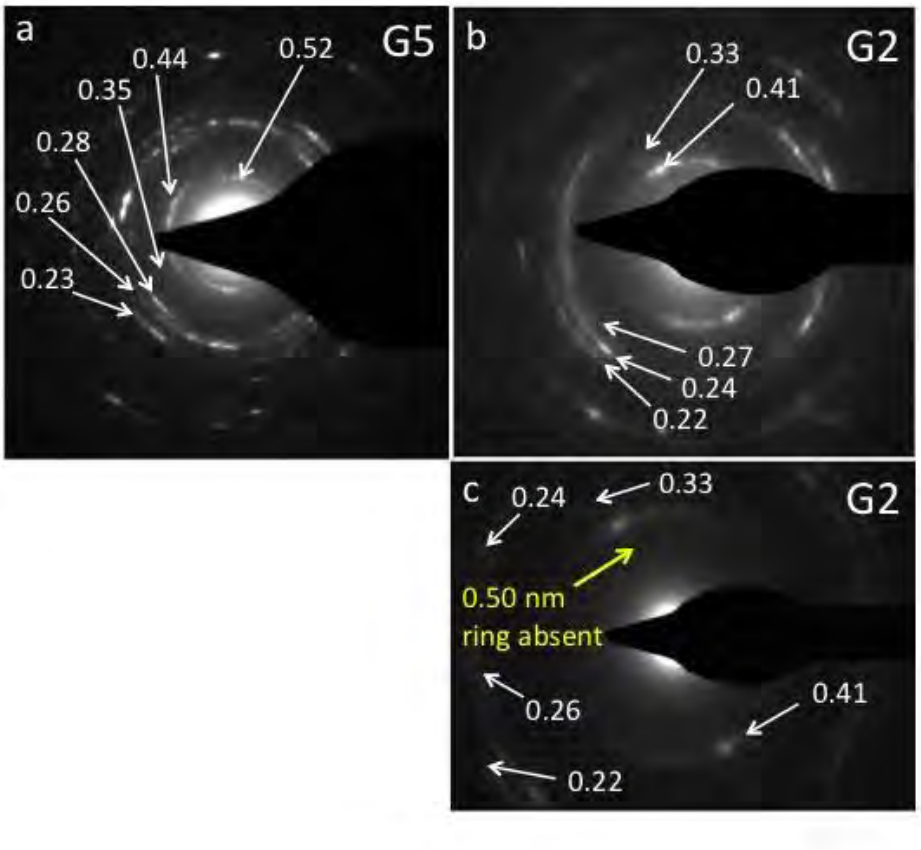

Figure 4

This is the peer-reviewed, final accepted version for American Mineralogist, published by the Mineralogical Society of America.
The published version is subject to change. Cite as Authors (Year) Title. American Mineralogist, in press.
DOI: https://doi.org/10.2138/am-2021-7768. http://www.minsocam.org/

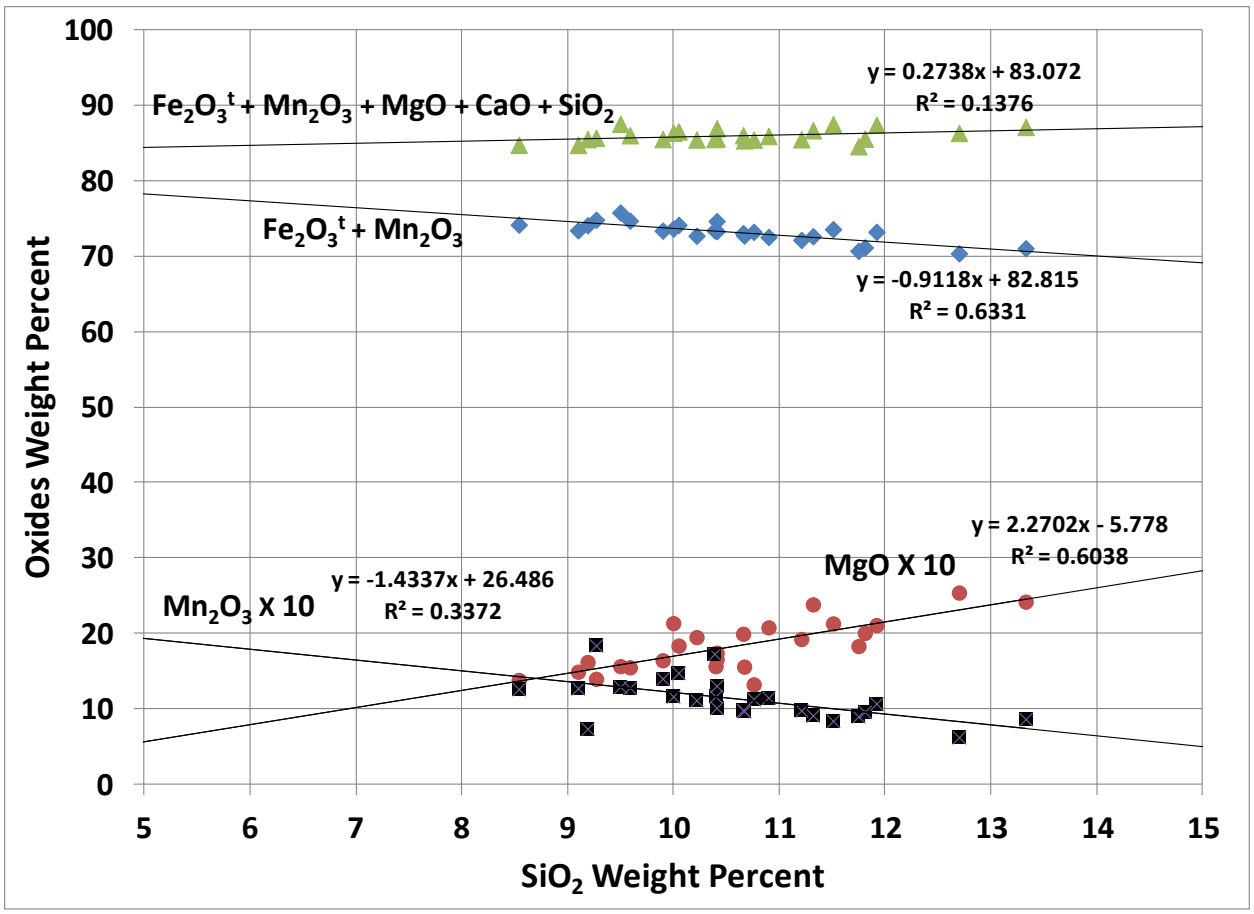

Figure 5

This is the peer-reviewed, final accepted version for American Mineralogist, published by the Mineralogical Society of America.
The published version is subject to change. Cite as Authors (Year) Title. American Mineralogist, in press.
DOI: https://doi.org/10.2138/am-2021-7768. http://www.minsocam.org/

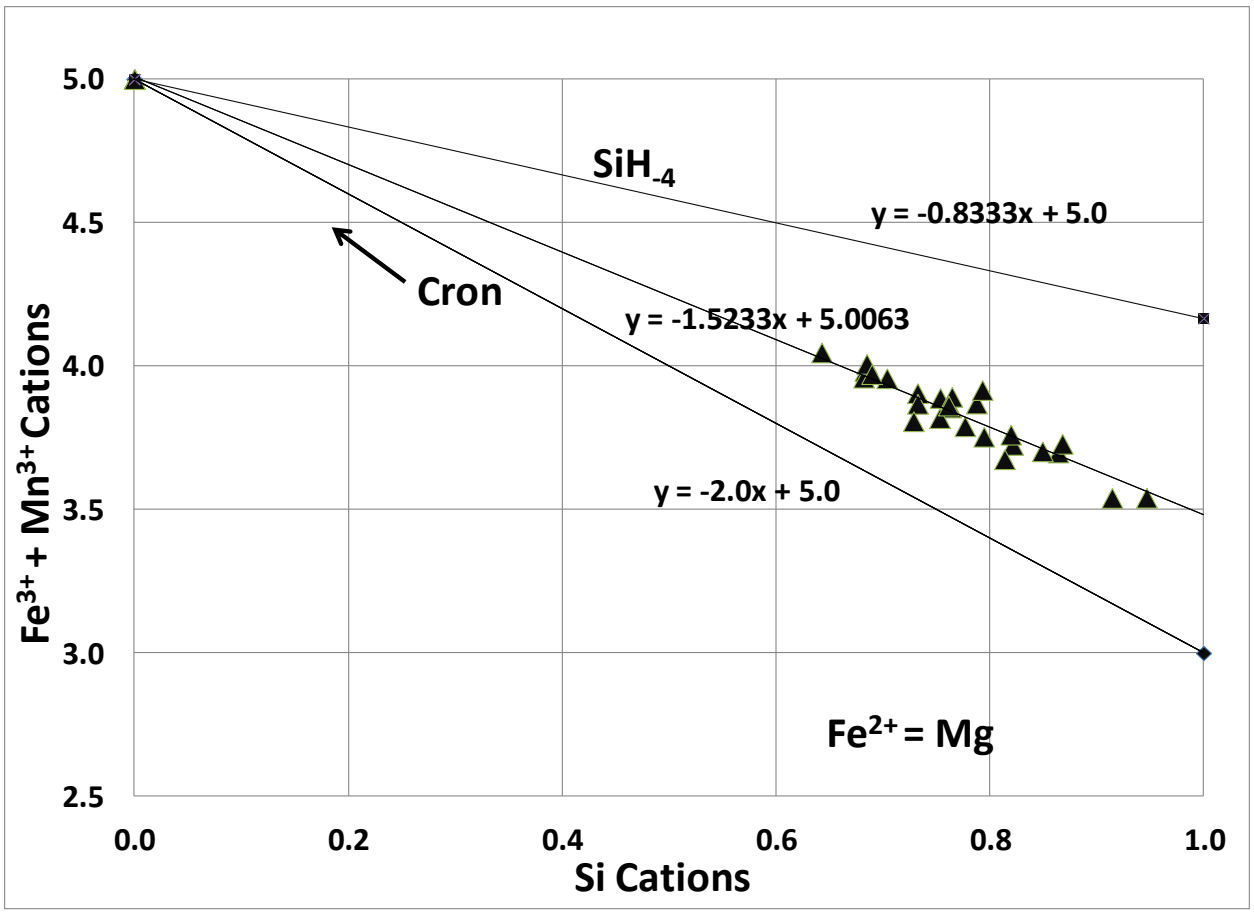

Figure 6

This is the peer-reviewed, final accepted version for American Mineralogist, published by the Mineralogical Society of America.
The published version is subject to change. Cite as Authors (Year) Title. American Mineralogist, in press.
DOI: https://doi.org/10.2138/am-2021-7768. http://www.minsocam.org/

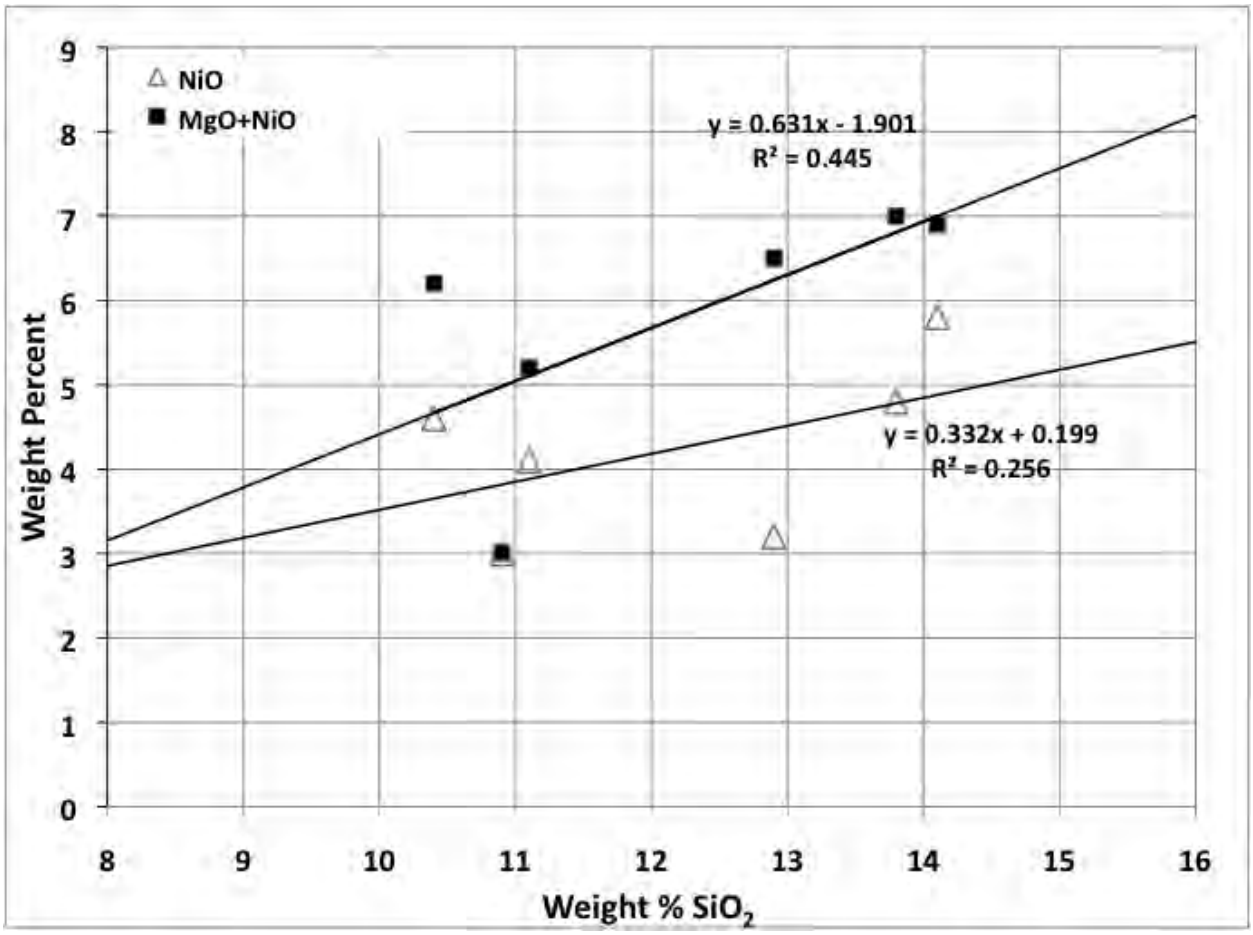

Figure 7

This is the peer-reviewed, final accepted version for American Mineralogist, published by the Mineralogical Society of America.
The published version is subject to change. Cite as Authors (Year) Title. American Mineralogist, in press.
DOI: https://doi.org/10.2138/am-2021-7768. http://www.minsocam.org/

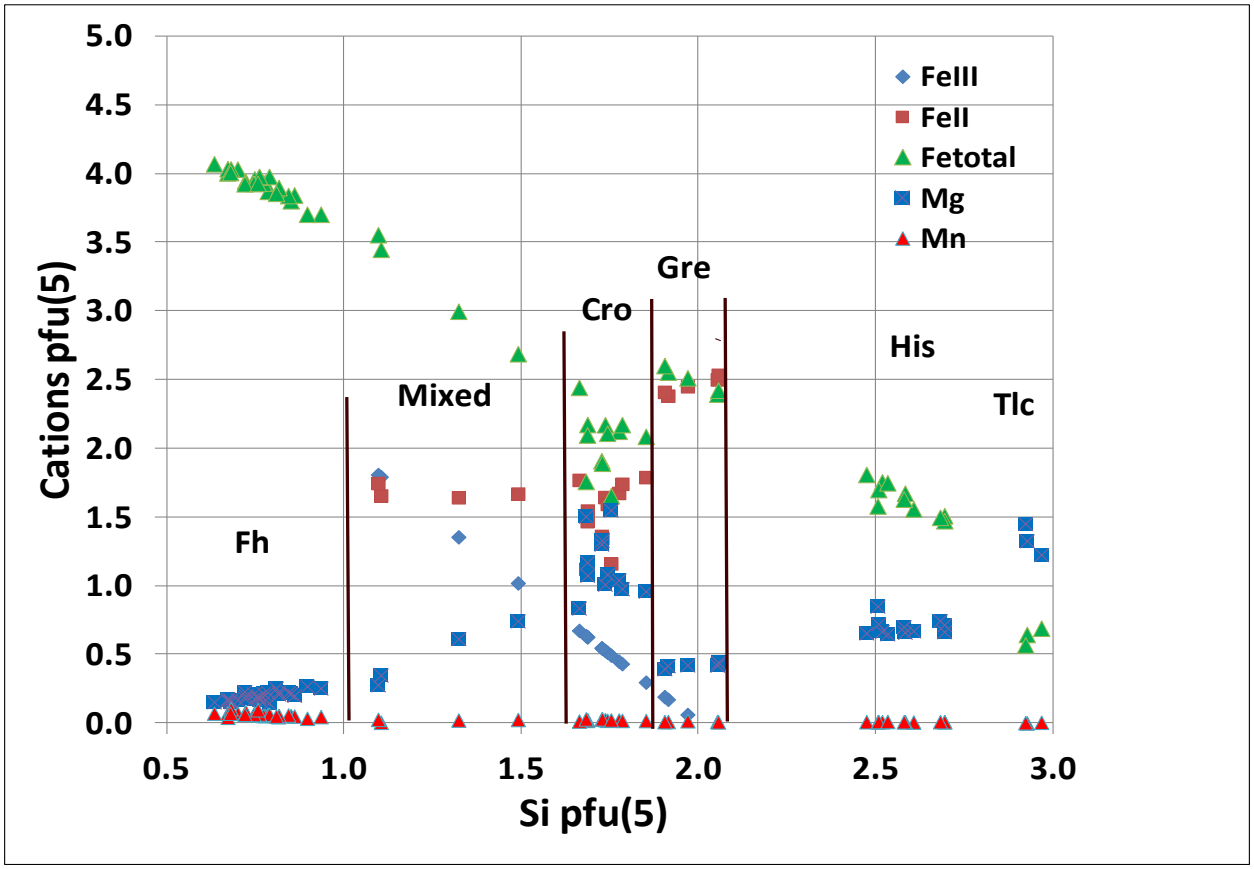

Figure 8

This is the peer-reviewed, final accepted version for American Mineralogist, published by the Mineralogical Society of America.
The published version is subject to change. Cite as Authors (Year) Title. American Mineralogist, in press.
DOI: https://doi.org/10.2138/am-2021-7768. http://www.minsocam.org/

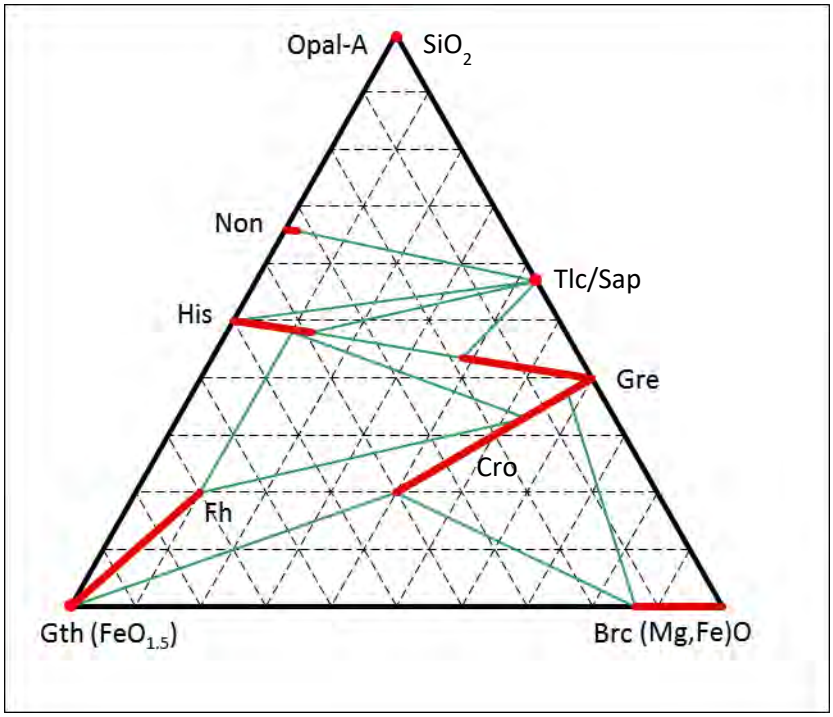

Figure 9